Computational fluid dynamics simulation of TPMS scaffolds for bone tissue engineering

Tiago Alexandre Hilário Veríssimo Pires
tiago.a.h.v.pires@tecnico.ulisboa.pt

Instituto Superior Técnico, Lisboa, Portugal

Abstract

Bones are a fundamental component of the human body given their multitude of functions. Thus, Bone Tissue Engineering has been focusing on improving the current methods for dealing with damaged bone. In this sense, the use of scaffolds has been presented as a possible alternative to traditional methods. Scaffolds are artificially designed porous support matrices, meant to allow cell seeding and cell proliferation. These properties are influenced by the permeability of the scaffolds. Taking this into consideration, this work used Computational Fluid Dynamics models to analyse the permeability and fluid streamlines of different TPMS scaffold geometries. The results from the simulations were used to better understand the relation between a scaffold's geometry and its permeability values. The computational models are also compared to an experimental setup in order to be validated. Because of the high computational cost to test the entire setup, three less demanding alternative models were designed. It was verified that the periodic model was the more appropriate, since it could be used for all of the designs keeping the original geometry. The results from the numerical analysis presented a good correlation with the experimental values, validating the computational models. The analysis of the fluid streamlines revealed how the gyroid geometries are the most appropriate design for most cases of scaffold fabrication. The study of the streamlines also showed that the Schwarz D geometries were only appropriate for very specific scenarios and the tested Schwarz P geometries did not possess the desired qualities for cell seeding and proliferation.

Key-words: Bone Tissue Engineering; Scaffolds; Permeability; Triply Periodic Minimal Surfaces; Computational Fluid Dynamics; Streamlines

1. Introduction

The primary support structure in the human body are the bones as described by *Tortora and Derrickson (2014)*. Bones perform a number of functions, which include structural support, protection and homeostasis. Considering the multitude of functions carried out by osseous tissues, any injury or defect on this tissue, which cannot be easily repaired, (that can be pathological, traumatic or surgical in nature), represents an issue that demands quick intervention. *Porter et al. (2009)* illustrates how the current standard for addressing these lesions is typically bone grafting, which consist of removing the damaged bone and replacing it with healthy tissue. However, because of the current limitations of bone grafting, Bone Tissue Engineering (BTE) has been researching the creation, utilization and optimization of scaffolds. These scaffolds are artificially designed porous support matrixes, meant to allow cell seeding and cell proliferation.

The motivation for the work is further encourage the use of scaffolds as a viable alternative to bone grafts in BTE. To achieve this, there is a need for more in depth studies to better understand one of the scaffold's most important characteristics: its geometry. This geometry is responsible not only for how much mechanical support the scaffold provides, but also for determining how cells will interact with it. Therefore, it's essential to understand how different geometries will influence all of the different scaffold properties.

To this end, this work will use a computational fluid dynamics (CFD) analysis will be used to simulate an experimental setup, in order to obtain the permeability of twelve distinct geometries. The permeabilities obtained

(alongside the flow streamlines of the CFD) will be compared between themselves to better understand how a change in a scaffold's geometry changes the fluid flow inside of it.

2. Background

When attempting to design a scaffold for BTE a fundamental factor to take into consideration is its permeability. This is because a scaffold's permeability will influence cell seeding, cell differentiation and cell growth, making it an essential parameter to consider in scaffold production. *Rahbari et al. (2016)* and *Dias et al. (2012)* discuss how higher scaffold permeability generates better conditions for cell growth inside them and how this permeability is dictated by the pore size and porosity of scaffolds. These studies also indicate how larger pore sizes and higher porosities lead to more permeable scaffolds. However, higher permeability in scaffolds is not without its limitations. *Melchels et al. (2010)* notes that when permeability is too high, all cells are able to pass through the scaffold, stopping cells adhering to its walls. Several different geometries have been considered when designing scaffolds for TE, for example, *Montazerian et al. (2017)* studied the permeability of several distinct geometries ranging from simpler lattice geometries to much more complex triply periodic minimum surfaces (TPMS). As expected, the TPMS structures always outperform the other designs (when comparing designs with the same porosity), revealing the benefits of choosing these geometries when attempting to optimize the permeability of scaffold meant for bone implantation. Accordingly, this work will be focussed on analysing scaffolds designed with the three most commonly studied TPMS geometries: Schwartz P, Schwartz D and gyroid. Schwarz P, as indicated by their name, is one of the simplest TPMS geometry, being approximated by the following equation *(Dinis et al., 2014)*:

$$\cos(x) + \cos(y) + \cos(z) = 0 \quad (1)$$

Schwarz D is a fairly more complex geometry that can be approximated by the following equation:

$$\sin(x) * \sin(y) * \sin(z) + \sin(x) * \cos(y) * \cos(z) + \cos(x) * \sin(y) * \cos(z) + \cos(x) * \cos(y) * \cos(z) = 0 \quad (2)$$

The third considered geometry for this work was the gyroid geometry. This is the most complex out of all three geometries because it possesses neither planar symmetries nor any straight lines, being composed of curved surfaces. It is approximated by:

$$\cos(\mathrm{x}) * \sin(\mathrm{y}) + \cos(\mathrm{y}) * \sin(\mathrm{z}) + \cos(\mathrm{z}) * \sin(\mathrm{x}) = 0 \quad (3)$$

These geometries are illustrated in Figure 1.

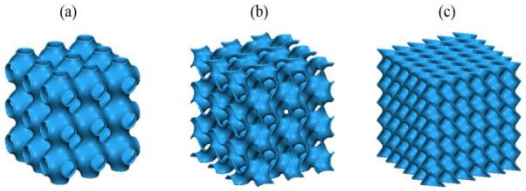

Figure 1. Illustration of a 3x3 a) Schwarz P geometry, b) gyroid geometry and c) Schwarz D geometry (Vijayavenkataraman et al., 2018).

These geometries were created using a custom program *(Dinis et al., 2014)* which, given the geometry and desired parameters, returns the geometry of a basic cubic unit of the scaffold, its porosity and a mesh of cubic hexahedral elements.

The basis for solving the numerical simulations and calculating the scaffold's permeability were the Navier-Stokes equations and Darcy's law. Darcy's law can be expressed as *(Jones, 1962)*:

$$\mathrm{K} = \frac{\mathrm{Q} * \mu * \mathrm{L}}{\mathrm{A} * \Delta \mathrm{P}} \quad (4)$$

where, K is the permeability expressed in m^2; $\Delta \mathrm{P}$ is the pressure drop before and after the section under study expressed in Pa; L is the length of the section or the test sample expressed in m; A is the cross sectional area of the flow expressed in m^2; μ is the dynamic viscosity of the fluid expressed in Pa*s and Q is the flow rate expressed in m^3/s. This equation has been an essential tool in determining the permeability of porous mediums and recently it has been used to determine the permeability of scaffolds (these are treated as an analogous of a porous medium), such as in *Dias et al. (2012)* and *Mohee et al. (2019).* However, Darcy's law can only be applied to laminar flow for a fluid with constant viscosity, which is why before applying this law we must determine the Reynolds number of the flow. The Reynolds

number is a dimensionless parameter given by:

$$\mathrm{Re} = \frac{\rho * \mathbf{U} * \mathrm{D}}{\mu} \quad (5)$$

where ρ is the fluid density; $\mathbf{U}$ is the velocity of the fluid and D is the diameter of the pipe. This variable determines the type of fluid flow, with the flow being laminar at lower Reynolds number and turbulent at higher numbers. *Ochoa et al. (2009)* and *Chor and Li (2006)* discussed how applying Darcy's law is only correct for a Reynolds number equal or lower than 1 with Re values up to 8.6 giving a insignificant variation.

3. Methods

3.1. Model Geometry

The computational setup was based on the experimental setup used in *Castro et al. (2019)*. The main component to represent in the numerical analysis was the permeability chamber, more specifically, the inside of the chamber (as a CFD analysis simulates only the fluid phase and not the actual chamber). However, representing the entire permeability chamber resulted in a large amount of space in the cylinders which was irrelevant for the numerical simulation. Therefore, it was decided to model the chamber with a smaller transversal squared area with 13 mm sides, as a way to the reduce the computational weigh of the simulations. This new model was a chamber with a squared cross section with 13 x 13 mm with the same total length of 77 mm (Figure 2).

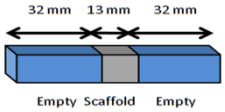

Figure 2. Representation of the CFD chamber with its dimensions.

For creating the mesh of the scaffolds, the previously mentioned program developed by *Dinis et al. (2014)* was used. The program returns .inp files (input files for the ABAQUS software) that represent the unitary cell of both the scaffold and the fluid phase with a cubic hexahedral mesh. The number of elements per side for a unitary cube is a required parameter of the software and it was determined that a minimum of forty elements per side was necessary to obtain a valid scaffold. The configuration of the final scaffold, was decided to be a 4 x 4 x 4 cubic scaffold with a 13 mm side (meaning each unitary cubic cell is a 3.25 mm sided cube and the mesh is constituted by 0.08125 mm side cubes), in order to follow the scaffold shape tested in *Castro et al. (2019)*. For this work, three different TPMS geometries were considered (SP, SD and SG) with four different levels of porosity for each of them (50%, 60%, 70% and 80% porosity). There are a total of twelve distinct scaffolds that will be henceforth be referred to by their geometry and porosity. For example, a SP scaffold with 70% porosity will be called SP70.

Having obtained a singular unitary cell with both phases (scaffold and fluid), a Matlab program was created that isolated the desired phase (in this case, the fluid phase), removing all of the nodes and elements of the mesh not being utilised. Afterwards, the program multiplies the fluidic unitary cell and combines the copies into the desired 4 x 4 x 4 shape. Finally, it attaches an empty chamber, before and after the scaffold, to simulate the permeability chamber. In order to maintain consistency through the simulation, the empty chambers were also mesh using 0.08125 mm sided cubes.

3.2. Numerical Models

The chosen software for conducting the CFD analysis was the 16.2 ANSYS FLUENT Solver. This commercial program consists on a FVM with the application of iterative methods to solve the previously discussed Navier-Stokes equations. This CFD solver has already proven its effectiveness in scaffold analysis such as described *by Ali and Sen (2018)* and *Marin and Lacroix (2015)*.

However, it was determined that the establish mesh parameters made it impossible to run the numerical analysis with the entire chamber and scaffold. A complete model would be made out of approximately 24 million elements (even when considering the simplified chamber) and the software was unable to run the model. Therefore, three alternative models were designed, which were the periodic model, the symmetric model and the simplified model. These models assume the fluid is flowing in the z direction, on a xyz coordinate system.

The first alternative model to be designed was one that took advantage of the nature of the TPMS geometry, namely the fact that it's

periodic. These periodic models assumed the scaffold being tested did not have a 4 x 4 x 4 configuration, but instead a 1 x 1 x 4 configuration with an infinite amount of unitary cells in both directions parallel to fluid flow (x and y). This would make it possible to model a simpler scaffold and chamber with 1/16 of the number of elements. These models ignore the effects of the walls of the chamber and focuses on determining the permeability of four cell deep scaffold. The main problem with these models is precisely the fact that, ignoring the effect of the chamber walls, will always wield a considerable higher permeability value than what would be observed in an experimental setup. For the implementation of this periodic model, a periodic boundary condition of FLUENT ANSYS was chosen. However, this condition requires that two boundaries with an equal shape are chosen, which could only be done in the SP scaffolds. To overcome this problem, a Matlab routine was created, designed to cut all the elements along the edge of the model in half, extract the outer half and place it on the opposite side of the model (Figure 3). This routine would guaranty that both sides have a boundary with the same shape. This program was applied on both the xz oriented faces and the yz oriented faces.

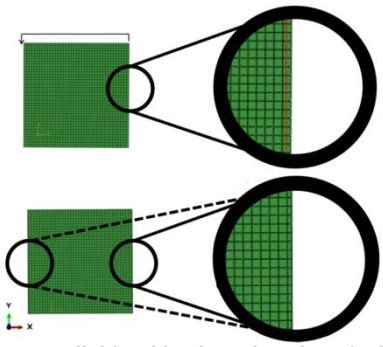

Figure 3. Scaffold with the chamber before the routine (top) and after the routine (bottom).

Another considered alternative was a model with two symmetry axis running through the middle of the chamber in the xz and yz orientation. However, contrary to the periodic model, this model is only valid if two conditions are met: the geometry has to have two symmetry axes in its middle and the fluid flow cannot pass through the symmetry axis. The second condition cannot be determined without first running the simulations, guarantying the fluid does not pass the boundary, thus validating this condition. However, the first condition can be validated *apriori*, only being valid for SP geometries, seeing as the other two do not possess any symmetry axes. Although TPMS geometries are necessarily periodic this does not mean they are necessarily symmetric.

The final alternative model that was designed was a simplified model with twenty elements per unitary cell instead of forty. This model goes against the condition established in the beginning of having a minimum of forty elements per unitary cell; however, because of the large number of total elements, it is the only method that allows the entire chamber to be represented.

4. Results

For all of the models, a total of eleven different inlet flow rates were studied between 1 and 100 ml/min. The velocities used on the numerical program were calculated based on the corresponding inlet flow rates (in m^3/s) and the constant cross sectional area of 0.000169 m^2. Finally, the conversion from pressure drop was made using Darcy's law with a length of 0.013 m, the mentioned area of 0.000169 m^2 and a dynamic viscosity of 0.001 Pa.s.

4.1. Symmetric models

Before measuring the pressure drop of any symmetric scaffold, the first step was verifying the previously discussed criteria for applying the symmetry boundary, namely that no flow goes through the symmetry plane. Studying the streamlines of the fluid flow (Figure 4), it could be observed that the flow in a SP geometry in the symmetry plane (right side) never crosses from one side to another.

The measurements of the calculated permeability for the symmetric scaffolds are shown in Figure 5.

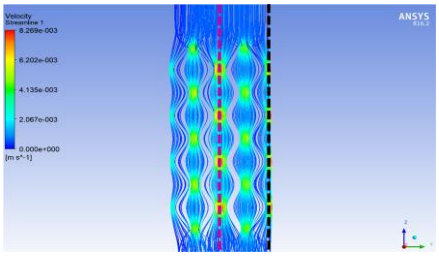

Figure 4. Streamlines for a SP70 scaffold with an inlet velocity of 5 ml/min, with a symmetry boundary condition in the right side.

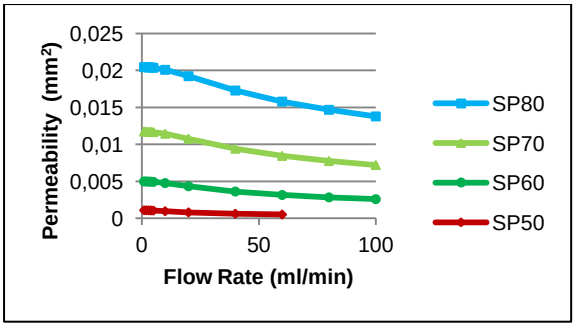

Figure 5. Calculated permeability in function of the flow rate for all of the four symmetric scaffold models.

As expected, there were higher permeability values for the scaffolds with the highest porosity; however, these values started to decrease at a flow rate of around 20 ml/min, signalling the point where the flow starts to exit the domain of Darcy's law. Nevertheless, this law is still applicable for the analysis of the fluid flow. Finally, for the flow rates of 80 and 100 ml/min, the numerical simulation did not converge for the SP50 scaffold, signalling the occurrence of a turbulent flow instead of the laminar flow expected by the software. Because of this, no results could be obtained for those two simulations.

4.2. Periodic models

The calculated permeabilities for the periodic models are shown in Figure 6 and Figure 7. The results show that all of the periodic models also suffered the same drop in permeability that was seen in the previous chapter. However, this decline was much higher in the SP geometries and barely noticeable in the SD geometries (gyroid structures presented an intermediate decline when compared to the other two). Also similar to what has observed in the previous chapter, was that geometries of the same type with higher porosity always resulted in a higher permeability. Taking this into consideration, the order of the permeability of the scaffolds (from the lowest permeability to the highest) was: SP50 < SD50 < SD60 < SG50 < SP60 < SD70 < SG60 < SD80 < SP70 < SG70 < SG80 < SP80.

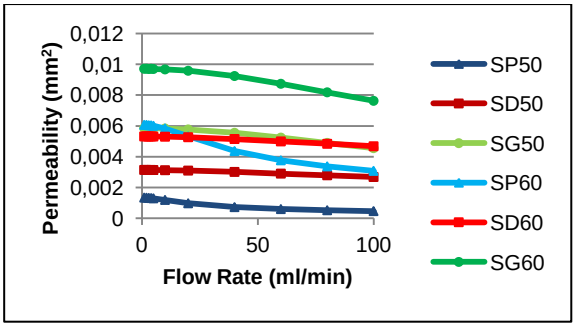

Figure 6. Calculated permeability in function of the flow rate for periodic scaffolds with 50% and 60% porosity.

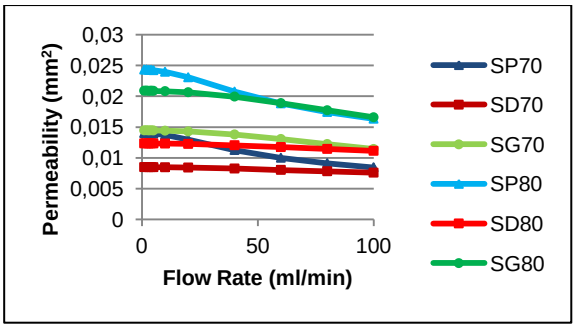

Figure 7. Calculated permeability in function of the flow rate for periodic scaffolds with 70% and 80% porosity.

When comparing the permeability values of the SP scaffolds from the periodic and symmetric models, there is a clear discrepancy. The permeabilities of the symmetric models were on average 16.7% lower to the periodic models. This is the aforementioned effect of the chamber wall, which causes a decrease in the permeability. To correct this, the approximation of the effect of the chamber wall of 16.7% was applied to all twelve periodic models (by multiplying all the calculated permeabilities by a correction factor of 0.833).

4.3 Simplified models

The calculated permeabilities for the simplified models are shown in Figure 8 and Figure 9.

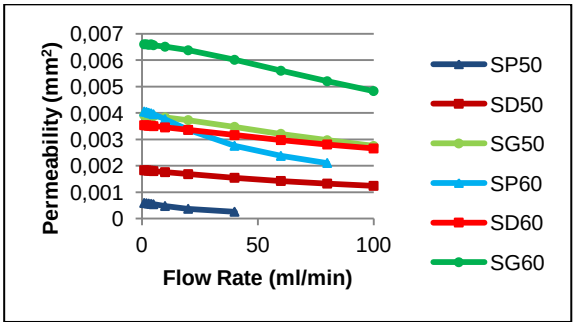

Figure 8. Calculated permeability in function of the flow rate for simplified scaffolds with 50% and 60% porosity.

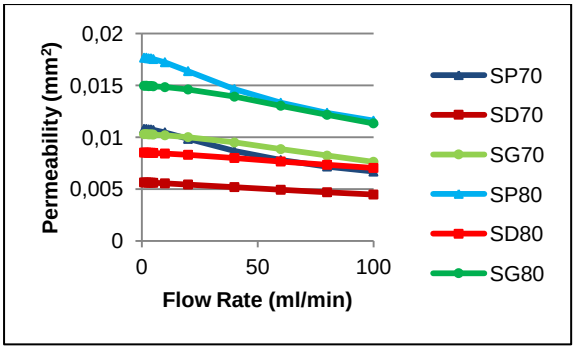

Figure 9. Calculated permeability in function of the flow rate for simplified scaffolds with 70% and 80% porosity.

4.4. Experimental Results

The experimental results include a selection of the porosities, namely 60% and 70% porous scaffolds, in order to evaluate the correlation between the experimental values and the numerical ones. They are represented alongside the corrected periodic models' values, for ease of comparison, in Figure 10 and Figure 11.

The experimental setup shows some inconsistencies at the flow rates smaller than 5 ml/min, caused by the sensitivity of the pressure transducer not being able to accurately measure the considerable small changes of pressure associated with those flow rates. Furthermore, the comparison between the experimental data with the numerical data reveals the numerical permeability values are between two to three times higher than the empirical values.

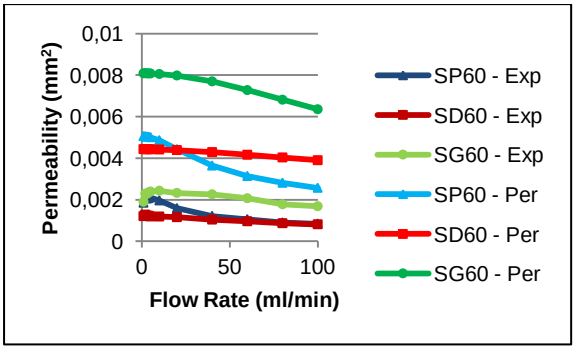

Figure 10. Calculated permeability in function of the flow rate for the experimental values (Exp) and corrected periodic values (Per) of scaffolds with 60% porosity.

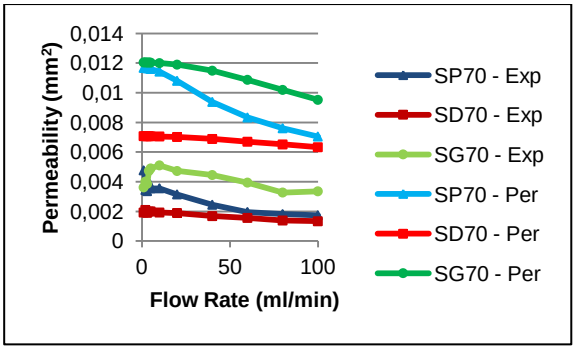

Figure 11. Calculated permeability in function of the flow rate for the experimental values (Exp) and corrected periodic values (Per) of scaffolds with 70% porosity.

5. Discussion

5.1. Permeability Analysis

The comparison between the corrected periodic model's permeabilities and the simplified model's permeabilities, shows that all of the simplified models always have a lower permeability to that of the corrected periodic model. This demonstrates how the inherent changes of the simplified model to the scaffolds geometry always results in a worse permeability. This raises a concern not only in computational tests, but also in experimental setups. As *Marin and Lacroix (2015)* previously found, changes in a scaffold's manufacturing process can greatly alter its fluidic properties. The results from the simplified models reveal how, similar to the imperfections in the printing process, small flaws in the simplified geometry will lead to a decrease in the scaffold's permeability. This means that besides the characteristics discussed by *Dias et al. (2012)* that influence a scaffold's permeability (pore size, porosity and permeability), there should also be a careful consideration of the refinement (the number of elements per side) of the CAD model being designed. These results reveal how, for the purpose of obtaining the optimal permeability values, the periodic model is preferable because it lacks the limitations of the simplified model and can be used for all TPMS geometries (unlike the symmetric models). In addition, because the periodic models represent fewer scaffold unitary cells, it is easier to observe and study the fluid flow inside it.

As was expected, the periodic models reveal how, for the same geometry, a lower porosity results in a lower permeability. However, when comparing different geometries, a lower porosity was not an assurance of a lower permeability. An example of this is how the SG50 has a higher permeability than the SD60 even though it has a lower porosity. The results ultimately show that only increases of at least 20% porosity guaranty an increase of the scaffold's permeability (all 50% porous scaffolds had lower permeability than the 70% scaffolds and all 60% porous scaffolds had lower permeability than the 80% scaffolds). The results support the view that even though porosity is the main factor in determining a scaffold's permeability, if it's coupled with the choice of geometry there can be greater control over the precision of the permeability. This is important, because the differentiation cells inside a scaffold is dependent on the velocity of the fluid passing through them and the shear strain they are under *(Castro and Lacroix, 2017)*. Therefore, being able to more precisely control a scaffold's permeability would allow better control of the differentiation of cells inside the scaffold (seeing as both shear stress and fluid velocity are related to permeability).

5.2. Streamline Analysis

The streamlines (Figure 12, Figure 13 and Figure 14) show that, for each model, there is not a singular path, but instead several paths with the same shape. These paths are: linear paths which expand in the interconnected areas for the SP scaffolds; circular helixes for the SG scaffolds and squared helixes for the SD scaffolds. Even though there are zones of connection between these paths, they never combine or separate. This means that there is always the same number of paths throughout the scaffold. Another observation was how the SP scaffolds was the only one of the scaffolds where there were large volumes without streamlines (indicating that when proceeding to cell seeding, the cells would not flow into these areas *(Marin et al., 2017*)). The volumes were the paths could have merged, which were perpendicular to the fluid flow, presented an appealing zone where the cells could be deposited and differentiated. But if the flow does not pass through these zones, then the cells could never interact with them, meaning there is a less overall area of interaction between the scaffold walls and cells.

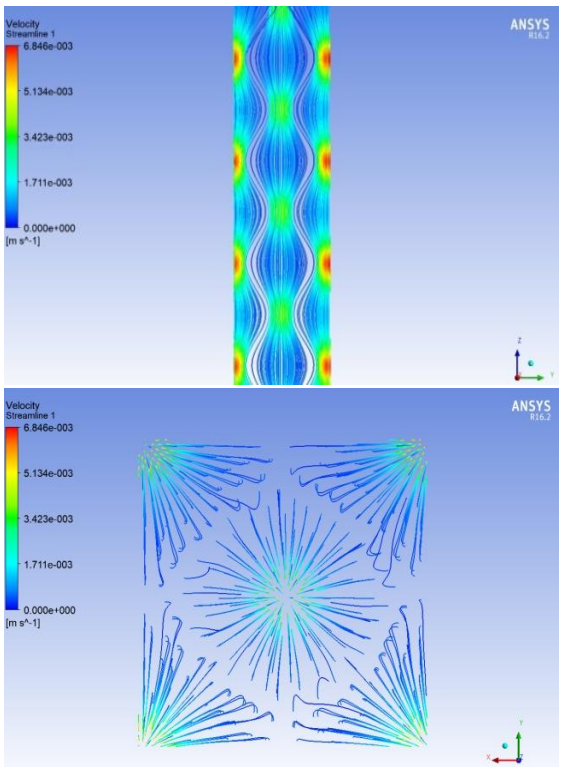

Figure 12. Side view (top) and oulet view (bottom) of the streamlines from a SP70 scaffold.

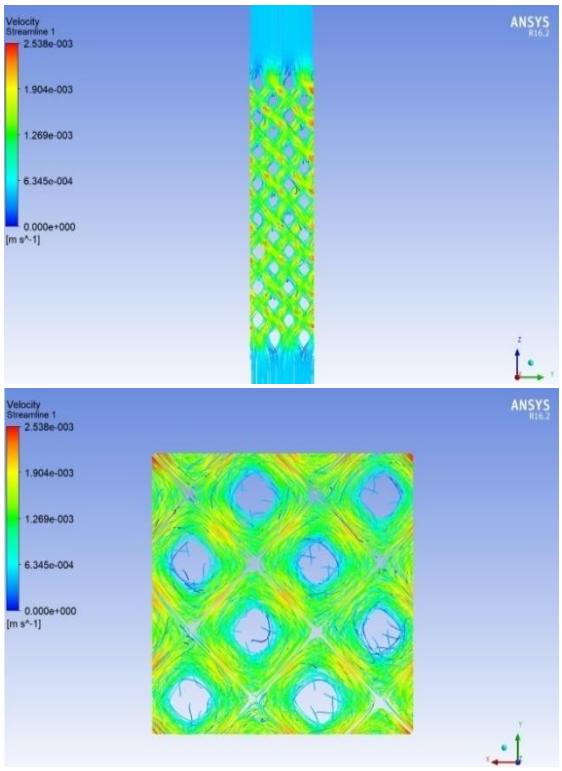

Figure 13. Side view (top) and oulet view (bottom) of the streamlines from a SD70 scaffold.

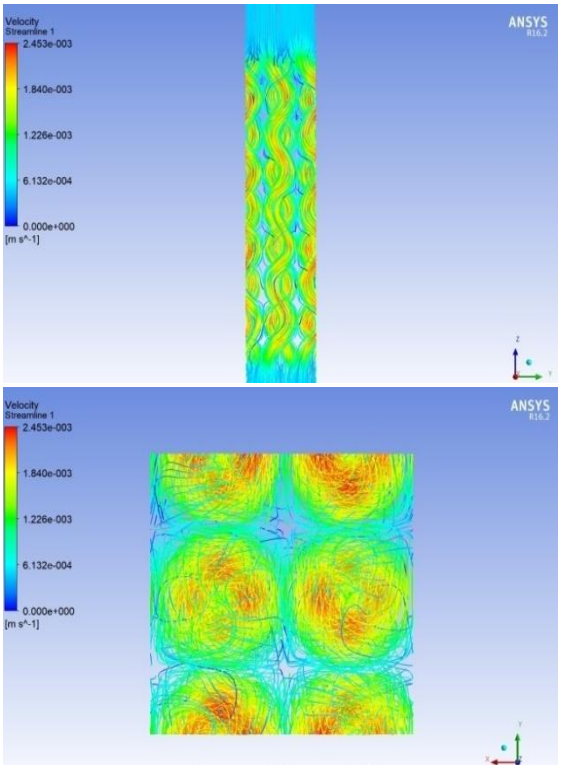

Figure 14. Side view (top) and oulet view (bottom) of the streamlines from a SG70 scaffold.

Other comparisons were made to observe how difference velocities and porosities influenced the streamlines for the three scaffolds. When comparing the streamlines for inlet flow rates between 5ml/min and 100 ml/min, there were no noticeable differences for either the SD or SG scaffolds, other than an overall increase of the velocity across the simulations. There were also no significant changes in the streamlines for these two geometries with changes in porosity, other than increase in velocity and narrower paths for lower porosities. However, when comparing these differences for the SP scaffolds, the distinctions were very apparent. The higher the inlet flow rate and the lower the porosity, the less volume is occupied by the streamlines inside the scaffold and the more length of the permeability chamber is required for the flow to stabilize. These occurrences explains why, in certain simulations of the SP50 at very high inlet flow rates, analysis was impossible (because of the instability of the flow, it was never laminar at the outlet).

In the end, all of the problems raised regarding the SP scaffolds stem from its design. The fact the flow is not forced into any change of directions and being able to travel in an almost straight line, means that the cells might pass the scaffold without interacting with it at all, rendering the entire purpose of the scaffold moot. In terms of the other two scaffolds, although both present paths that force the interaction between the flow and the scaffold walls, the design of the SD geometries causes the overall lowest permeability of all three scaffolds. This means the preferable option for scaffold design, that has both a high permeability and a travel path that leads the cells inside the flow to interact with the scaffold, is the Gyroid geometry. Nevertheless, the SD scaffolds presented the most stable permeability out of the three scaffolds regarding the increase in inlet flow rate. This means that the decrease in permeability for higher inlet flow rates was minimal for these scaffolds. Therefore, SD scaffolds might be the more preferable design in scenarios which involve fluids travelling at varying velocities and that have a need for a constant permeability.

5.3. Experimental comparison

The comparison between the experimental and numerical values reveals that all of the experimental permeability values are significantly lower than the numerical values. The numerical results are between two to three times higher than the experimental results. The comparison also showed how the experimental values were significantly inconsistent at inlet flow rates below 5 ml/min. This is due to the lack of precision of the pressure sensor for low pressure drops. Taking this into consideration, all of the experimental results for flow rates lower than 5 ml/min were disregarded.

In order to determine whether these two sets of permeability have a good correlation, a comparison was established between these two sets for each of the scaffolds. This comparison revealed, for each scaffold, a linear relation with an R^2 between 0.93 and 0.98, indicating a good correlation between both sets of results. A subsequent comparison that analysed all of the points as a whole (Figure 15), instead of separating them by scaffold, found a R^2 equal to 0.886, indicating high correlation between the sets.

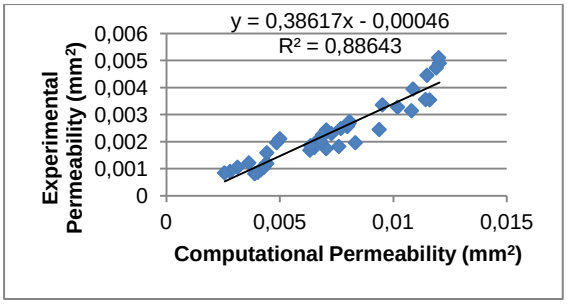

Figure 15. Correlation between the computationally calculated permeability and the experimentally measured permeability for all of the 60% and 70% scaffold porosities.

In a similar permeability study, *Dias et al. (2012)* also obtained a good correlation between the calculated and measured permeability values of their scaffolds (R^2 = 0.9172), but also registered calculated values much higher than the measured ones, approximately four times higher. *Dias et al. (2012)* raised some possible explanations behind these inconsistencies, such as the disregarded surface effects of the materials like their roughness and wettability.

Another component that could justify the difference in values is the manufacturing process. A scaffold's permeability can be greatly influence by small imperfections caused by the printing process *(Marin and Lacroix, 2015)*. Another possibility that could result in a change to the geometry is the wax that was used as the printing support material. This material might not have been correctly removed from the inside of the scaffolds, given the nature of the process, resulting in blockages to the fluid flow and decreasing the permeability. Finally, a factor that could also account for the decrease in permeability is how the permeability system was represented in the CFD model. Although the use of a squared permeability chamber instead of the full cylindrical chamber should not lead to a significant change in the permeability, a problem might arise from not representing the rubber pipes attached to the chamber (like it was considered).

6. Conclusion

The focus of this work was to better the understanding of the relation between a scaffold's design (geometry and porosity) and its permeability. To achieve this, three different TPMS geometries with four different porosities were tested, for a total of twelve different scaffolds. The values obtained from the numerical simulations were considered valid given their good correlation with experimental results, despite the differences between both sets of values (this was attributed to the simplifications of the numerical models and the imprecisions of the scaffold manufacturing process). Furthermore, the computational results were also were coherent with the findings of previous studies of TPMS scaffolds, regarding the permeability order of the different scaffolds designs.

The periodic models revealed much better results than the simplified models because they kept the original structure of the scaffold. However, the permeability values of the periodic models were higher than symmetrical models, most likely because of the lack of the effect of the chamber wall. To correct this, a correction factor of 0.833 was applied to all of the periodic models.

The analysis of the streamlines showed how the SP scaffolds were the ones most influenced by shifts in the porosity and inlet flow rate. Furthermore, because of the path that the fluid, and consequently the cells, would follow inside this scaffold, it was demonstrated that there was a limited interaction between these cells and the scaffold walls. Therefore, the SP geometry was revealed not to have the necessary qualities to promote cell seeding inside the scaffold. The SD scaffolds were determined as not to be a suitable geometry for most cases, unless there was a specific requirement for a scaffold with a constant permeability at various fluid velocities. Finally, the SG scaffolds had the overall highest permeability values and travel paths that promoted cell-scaffold interactions. Because of this, the SG geometry was recognized as the most advisable scaffold choice for most situations.

The results obtained throughout this dissertation underline the importance of numerical analysis and CFD models in the study of scaffolds with applications in BTE. Furthermore, several possibilities for further study around this subject emerged. These include analysing a complete model of the experimental setup and examining how the

number of elements per side of the scaffold models influences the permeability values.

References

Ali, D. and Sen, S. (2018). Permeability and fluid flow-induced wall shear stress of bone tissue scaffolds: Computational fluid dynamic analysis using Newtonian and non-Newtonian blood flow models. *Computers in Biology and Medicine*, 99, pp.201-208.

Castro, A. and Lacroix, D. (2017). Micromechanical study of the load transfer in a polycaprolactone–collagen hybrid scaffold when subjected to unconfined and confined compression. *Biomechanics and Modeling in Mechanobiology*, 17(2), pp.531-541.

Castro, Pires, Santos, Gouveia and Fernandes (2019). Permeability versus Design in TPMS Scaffolds. *Materials*, 12(8).

Chor, M. and Li, W. (2006). A permeability measurement system for tissue engineering scaffolds. *Measurement Science and Technology*, 18(1), pp.208-216.

Dias, M., Fernandes, P., Guedes, J. and Hollister, S. (2012). Permeability analysis of scaffolds for bone tissue engineering. *Journal of Biomechanics*, 45(6), pp.938-944.

Dinis, J., Morais, T., Amorim, P., Ruben, R., Almeida, H., Inforçati, P., Bártolo, P. and Silva, J. (2014). Open Source Software for the Automatic Design of Scaffold Structures for Tissue Engineering Applications. *Procedia Technology*, 16, pp.1542-1547.

Jones, K. (1962). On the differential form of Darcy's law. *Journal of Geophysical Research*, 67(2), pp.731-732.

Marin, A. and Lacroix, D. (2015). The inter-sample structural variability of regular tissue-engineered scaffolds significantly affects the micromechanical local cell environment. *Interface Focus*, 5(2).

Marin, A., Grossi, T., Bianchi, E., Dubini, G. and Lacroix, D. (2017). µ-Particle tracking velocimetry and computational fluid dynamics study of cell seeding within a 3D porous scaffold. *Journal of the Mechanical Behavior of Biomedical Materials*, 75, pp.463-469.

Marin, A., Grossi, T., Bianchi, E., Dubini, G. and Lacroix, D. (2017a). µ-Particle tracking velocimetry and computational fluid dynamics study of cell seeding within a 3D porous scaffold. *Journal of the Mechanical Behavior of Biomedical Materials*, 75, pp.463-469.

Mohee, L., Offeddu, G., Husmann, A., Oyen, M. and Cameron, R. (2019). Investigation of the intrinsic permeability of ice-templated collagen scaffolds as a function of their structural and mechanical properties. *Acta Biomaterialia*, 83, pp.189-198.

Montazerian, H., Zhianmanesh, M., Davoodi, E., Milani, A. and Hoorfar, M. (2017). Longitudinal and radial permeability analysis of additively manufactured porous scaffolds: Effect of pore shape and porosity. *Materials & Design*, 122, pp.146-156.

Ochoa, I., Sanz-Herrera, J., García-Aznar, J., Doblaré, M., Yunos, D. and Boccaccini, A. (2009). Permeability evaluation of 45S5 Bioglass®-based scaffolds for bone tissue engineering. *Journal of Biomechanics*, 42(3), pp.257-260.

Porter, J., Ruckh, T. and Popat, K. (2009). Bone tissue engineering: A review in bone biomimetics and drug delivery strategies. *Biotechnology Progress*, p.1539-1560.

Rahbari, A., Montazerian, H., Davoodi, E. and Homayoonfar, S. (2016). Predicting permeability of regular tissue engineering scaffolds: scaling analysis of pore architecture, scaffold length, and fluid flow rate effects. *Computer Methods in Biomechanics and Biomedical Engineering*, 20(3), pp.231-241.

Tortora, G. and Derrickson, B. (2014). *Principles of anatomy & physiology*. 14th ed. John Wiley & Sons, pp.170-175.

Vijayavenkataraman, S., Zhang, L., Zhang, S., Hsi Fuh, J. and Lu, W. (2018). Triply Periodic Minimal Surfaces Sheet Scaffolds for Tissue Engineering Applications: An Optimization Approach toward Biomimetic Scaffold Design. *ACS Applied Bio Materials*, 1(2), pp.259-269.